Integrated production of an influenza A vaccine candidate with MDCK suspension cells

Thomas Bissinger [1*], Yixiao Wu [1,2], Pavel Marichal-Gallardo [1], Dietmar Riedel [3], Xuping Liu [2], Yvonne Genzel [1], Wen-Song Tan [2], Udo Reichl [1,4]

[1] Bioprocess Engineering, Max Planck Institute for Dynamics of Complex Technical Systems, Magdeburg, Germany

[2] State Key Laboratory of Bioreactor Engineering, East China University of Science and Technology, Shanghai, China

[3] Facility for Transmission Electron Microscopy, Max Planck Institute for Biophysical Chemistry, Goettingen, Germany

[4] Chair of Bioprocess Engineering, Otto von Guericke University Magdeburg, Magdeburg, Germany

* Present address: Roche Diagnostics GmbH, Pharma Research and Early Development, Bioprocess Research, Penzberg, Germany.

Correspondence

Yvonne Genzel, Bioprocess Engineering Group, Max Planck Institute for Dynamics of Complex Technical Systems, Magdeburg, Germany.

Email: genzel@mpi-magdeburg.mpg.de

Xuping Liu, State Key Laboratory of Bioreactor Engineering, East China University of Science and Technology, Shanghai, China.

Email: xupingliu@ecust.edu.cn

Thomas Bissinger, Yixiao Wu and Pavel Marichal-Gallardo contributed equally to this work.

Keywords

influenza virus production, chemically-defined medium, upstream processing, membrane chromatography, downstream processing

Graphical abstract

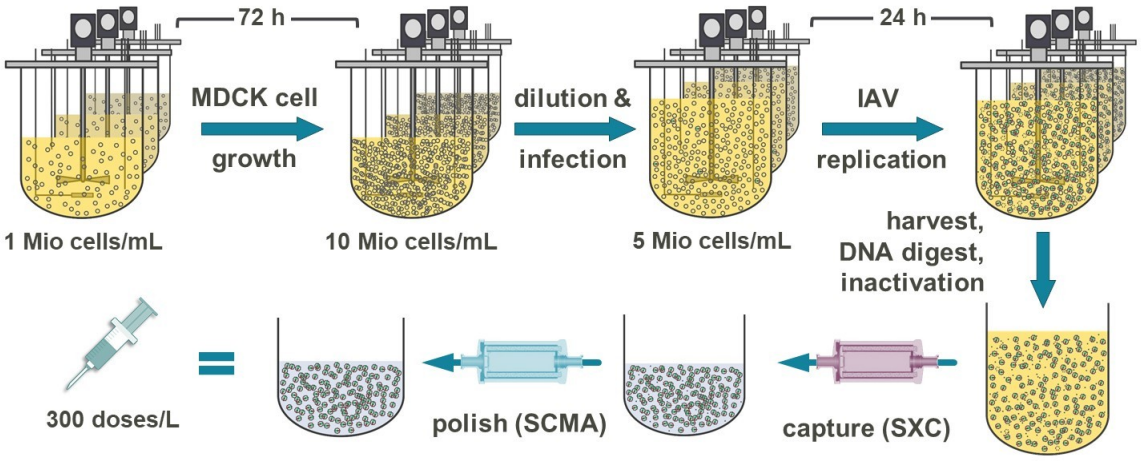

Abstract

Seasonal influenza infection waves occur both in northern and southern hemispheres every year. Despite the differences in influenza virus surface antigens and virulence of seasonal subtypes, manufacturers are well-adapted to respond to this periodical vaccine demand. Due to decades of influenza virus research, the development of new influenza vaccines is relatively straight-forward. Nevertheless, compared to the recent Covid-19 pandemic where a vaccine is not yet available, influenza vaccine manufacturing would be a major bottleneck for the rapid supply of billions of doses required worldwide. In particular, egg-based vaccine production would be difficult to schedule and shortages of other egg-based vaccines with high demands also have to be anticipated. Cell culture-based production systems enable manufacturing of large amounts of vaccines within a short time frame and expand significantly our options to respond to pandemics and emerging viral diseases. In this work, we present an integrated process for the production of inactivated influenza A virus vaccines based on a MDCK suspension cell line cultivated in a chemically defined medium. Very high titers of 3.6 $\log_{10}$(HAU/100 µL) were achieved using fast growing MDCK cells at concentrations up to 9.5 × 10^6 cells/mL infected with influenza A/PR/8/34 H1N1 virus in 1 L stirred tank bioreactors. A combination of two membrane-based chromatography steps enabled full recovery for the virus capture and up to 80 % recovery for the virus polishing step, respectively. Purified virus particles showed a homogenous size distribution around a mean diameter of 80 nm. Based on a monovalent dose of 15 µg hemagglutinin (SRID assay), the level of total protein was 58 µg and the level of host cell DNA contamination was below 10 ng. Furthermore, all process steps can be fully scaled up to industrial quantities for commercial manufacturing of either seasonal or pandemic influenza virus vaccines. Fast production of up to 300 vaccine doses per liter within 4 to 5 days makes this process competitive not only to other cell-based processes, but to egg-based processes as well.

Introduction

As for COVID-19, influenza A virus (IAV) pandemics pose an unpredictable threat both for human health and global economies (Horimoto & Kawaoka, 2001; Kilbourne, 2006; K. S. Li et al., 2004). Several of the highly infectious IAV subtypes have the potential to develop pandemic strains spreading rapidly around the globe, causing severe damage to humans and animal livestock (Webby & Webster, 2003). Even though no influenza pandemic has been reported since 2009, preparedness to fight future local or global epidemics is needed (Fineberg, 2014; Girard, Tam, Assossou, & Kieny, 2010; Webby & Webster, 2003). In case of a pandemic, vaccination will be the major control strategy to protect healthy individuals and to prevent further IAV distribution (Ferguson et al., 2006; Kostova et al., 2013). In such a scenario, billions of vaccine doses would be required at very short notice. Approved vaccines to battle seasonal influenza outbreaks come in three major formulations: live attenuated virus, inactivated virus (whole virus, split virus, viral subunit), and recombinant viral surface antigen (hemagglutinin) (Bresee, Fry, Sambhara, & Cox, 2018; Jin & Subbarao, 2015). Inactivated virus vaccines present the absolute majority (>98 %) of production capacity (Barr et al., 2018), thus playing the major role in vaccine manufacturing for a pandemic scenario. Here, either embryonated chicken eggs (ECE) or animal cells can be used as substrate for influenza virus propagation. Even though egg-based flu vaccines dominate the seasonal vaccine manufacturing, they are considered less suitable for pandemic influenza vaccine production (Audsley & Tannock, 2004). Apart from common disadvantages like long lead times for start of manufacturing, poor scalability and limitations in ECE supply (Genzel & Reichl, 2009), egg derived vaccines might be less protective against some influenza virus strains (Raymond et al., 2016; Schild, Oxford, de Jong, & Webster, 1983; Skowronski et al., 2014; Wu et al., 2017; Zost et al., 2017). In addition, ECE are being used for a number of other vaccines, i.e. to protect against yellow fever where frequent vaccine shortage has been reported (CDC, 2020). In contrast, animal cell culture platforms are highly flexible, versatile, easily scalable and can be very productive (Ernest & Kamen, 2015; Gallo-Ramirez, Nikolay,

Genzel, & Reichl, 2015). Especially with the application of single use equipment, small production facilities could generate pandemic vaccines rapidly in the location of need (Coronel et al., 2019; George et al., 2010; Lopes, 2015). Several adherent and suspension cell lines were evaluated for influenza vaccine manufacturing, and among these, adherent Madin-Darby Canine kidney (MDCK) cells remain the most productive cell line (Genzel & Reichl, 2009). MDCK cells are easily accessible (Dukes, Whitley, & Chalmers, 2011), widely used in influenza research and already licensed successfully for vaccine manufacturing (Doroshenko & Halperin, 2009). For MDCK cells growing in suspension, however, disadvantages like low specific growth rate, low cell concentration and unwanted formation of cell aggregates have been reported (Castro et al., 2015; Chu, Lugovtsev, Golding, Betenbaugh, & Shiloach, 2009; Lohr, Genzel, Behrendt, Scharfenberg, & Reichl, 2010; van Wielink et al., 2011). More recently, medium development led to fast growing MDCK suspension cell lines with the capability to grow as single cells to concentrations exceeding 10×10^6 cells/mL (Bissinger et al., 2019; D. Huang et al., 2015; Wang et al., 2017). For large scale manufacturing, both fast cell growth and high maximal cell density are crucial in order to reduce time to reach the needed production scale.

Besides production, virus particle purification plays a major role for the manufacturing of safe cell culture-based influenza vaccines (Onions, Egan, Jarrett, Novicki, & Gregersen, 2010). Biopharmaceutical products have to be purified to extremely high standards. Techniques for downstream processing (DSP) of virus particles at industrial scale typically involve filtration and chromatography methods (Wolf & Reichl, 2011). Examples of the latter are ion exchange chromatography (IEX) (Lee, Chan, Tan, Tam, & Tey, 2015; Vajda et al., 2016), size exclusion chromatography (SEC) (Kröber, Wolff, Hundt, Seidel-Morgenstern, & Reichl, 2013; Ruining WANG, 2015), hydrophobic interaction chromatography (HIC) (H. Li et al., 2015; Michael W. Wolff, Siewert, Hansen, Faber, & Reichl, 2010), affinity and pseudo-affinity chromatography (B Carvalho et al., 2018; A. R. Fortuna, Taft, Villain, Wolff, & Reichl, 2018), and multimodal chromatography (Baek, Seo, Kim, & Kim, 2011; Kuiper, Sanches, Walford, & Slater, 2002). Standard unit operations, like depth filtration, (ultra-)centrifugation,

(ultra-)filtration and column chromatography are generally combined to build a DSP train (Morenweiser, 2005; Wolf & Reichl, 2011; M. W. Wolff & Reichl, 2008). Chromatography resins are porous bead-based stationary phases that have diffusional limitations and other mass transport disadvantages for purification of large biomolecules (i.e. viruses) ("Chromatographic Purification of Virus Particles," ; P. Gagnon, 2009). In contrast, matrices with micron-sized flow channels that favor convective mass transport such as membranes and monoliths are much better suited for the purification of virus particles. Especially membrane-based chromatography materials are relatively inexpensive and allow single use applications. Membrane-based steric exclusion chromatography (SXC) has been reported for the purification of IAV (Marichal-Gallardo, Pieler, Wolff, & Reichl, 2017). SXC is performed by mixing an unpurified solution containing virus particles with polyethylene glycol (PEG) and feeding this mixture into a chromatography column whose matrix consists of disposable cellulose membranes. The virus particles are captured on the membrane surface without a direct chemical interaction, while smaller impurities are washed away. Selectivity in SXC is strongly based on the size of the target product and different influenza virus strains can be purified using the same process conditions. Unlike most other chromatography methods, in SXC the virus particles are loaded and eluted at physiological pH and salt concentrations that do not compromise the biological activity of the product. SXC can be complemented with pseudo-affinity chromatography like sulfated cellulose membrane adsorbers (SCMA) (A. R. Fortuna et al., 2018). Both SCMA and SXC have very high binding capacities and a high recovery of influenza virus particles, what makes them perfect candidates for capture or polishing unit operations, respectively (A. R. Fortuna et al., 2018; R. A. Fortuna et al., 2019; Marichal-Gallardo et al., 2017; Opitz, Lehmann, Reichl, & Wolff, 2009).

Although plenty of reports exist for either the production or the purification of cell culture-based influenza viruses, few integrated processes have been described in detail (Aggarwal, Jing, Maranga, & Liu, 2011; Genzel, Fischer, & Reichl, 2006; Hu et al., 2011; Montomoli et al., 2012; Tree, Richardson, Fooks, Clegg, & Looby, 2001; Weigel et al., 2016). Moreover, despite many advantages of cell culture-based influenza vaccine manufacturing the

application is still quite limited. This might be due to high costs of process development, limitations of suitable cell lines for large scale manufacturing, the lack of technological expertise, or extremely high costs involved in clinical testing of vaccine candidates. To overcome the technical limitations, careful analysis is crucial to demonstrate integrated process performance, robustness and productivity. In this study, we present a workflow for integrated cell culture-based production and purification of an inactivated influenza vaccine candidate that involves cultivation of MDCK suspension cells in three parallel lab-scale stirred tank bioreactors in chemically-defined medium and infection of cells with the influenza virus A/PR/8/34 H1N1 strain. We show the dynamics of cell growth, metabolism and virus replication, the identification of the optimal harvest point, and a purification train including enzymatic digestion of the host cell DNA and membrane-based chromatography of harvested virus particles by capture with SXC and polishing with SCMA. Additionally, we examine intermediate process steps such as the chemical inactivation of virus particles and discuss the selection and combination of these unit operations for the whole process. Very detailed analytics are applied to analyze the integrated process with a comprehensive dataset.

Overall, we demonstrate a comprehensive integrated platform technology with high potential for timely and fast large-scale manufacturing of pandemic influenza virus vaccines.

Material and Methods

Cell lines & cell culture

A MDCK suspension cell line (ATCC CCL-34 origin) generated previously (D. Huang et al., 2015; Ding Huang, Zhao, & Tan, 2011), was adapted to a newly developed chemically defined medium, referred as “Xeno-CDM” (Shanghai BioEngine Sci-Tech, Shanghai, China). MDCK suspension cells in Xeno-CDM were growing as single cell suspension to maximal cell concentrations (batch) of up to 12 × 10^6 cells/mL. For small scale cultivation, MDCK cells were grown in shake flasks (125/250 mL polycarbonate Erlenmeyer flask, #431143/#431144, Corning®, Corning, USA) with 30/60 mL working volume (wv) in a Multitron Pro incubator (Infors HT, Bottmingen, Switzerland) at 37 °C and 5 % CO_2 atmosphere with a shaking frequency of 100 rpm. Cells were passaged every three days with a seeding density of 0.5 × 10^6 cells/mL. Cell concentration, cell diameter, and cell viability were measured with a Vi-CELL XR automated cell counter (#731050, Beckman Coulter, Pasadena, USA). The average cell volume was determined from the diameter size distribution (class width 0.31 µm) of the analyzed population (2,000–15,000 cells) assuming a spherical cell shape. The viable cell volume (VCV) was calculated from average cell volume and viable cell concentration (VCC). For process evaluation, MDCK cells were cultivated in DASGIP® Bioreactors (#76DS0700ODSS, Eppendorf, Hamburg, Germany) with 300–600 mL wv. Approximately 50 mL of independent precultures (Erlenmeyer flask, 60 mL wv, 8–9 × 10^6 cells/mL) were used to inoculate each bioreactor (STR1-3) with an initial wv of 400 mL at a cell concentration of 1 × 10^6 cells/mL. All bioreactors were controlled by a DASGIP® Parallel Bioreactor System (#76DG04CC, Eppendorf, Hamburg, Germany) using the DASware® control software (#76DGCS, Eppendorf, Hamburg, Germany). A macrosparger with an air-oxygen mixture was used for aeration. The pH was controlled by CO_2 flow to the sparger and by addition of 1 M NaOH. For agitation, a single 30° pitched 3-blade stirrer (O.D. 50 mm) was used at a stirring speed of 80 rpm.

Influenza virus infection

All infections were carried out using an influenza A seed virus strain A/PR/8/34 of the subtype H1N1 from the Robert Koch Institute (Berlin, Germany), named here thereafter either “IAV” or “APR8”. The original seed virus propagated in adherent MDCK cells (#84121903, ECACC, Public Health, Salisbury, UK) was adapted over five passages (MOI 10^{-5}) to the MDCK suspension cell line. For infection, MDCK cells were diluted by half with fresh Xeno-CDM with trypsin addition (final activity 30 U/mL; #27250018, Thermo Fisher Scientific, Waltham, USA). Seed virus (infectious titer of 1.8×10^9 $TCID_{50}$/mL) was diluted with PBS and added to the cell suspension with a multiplicity of infection (MOI) of 10^{-3}.

Harvest and chemical inactivation of virus particles

A volume of 50 mL of cell suspension from each bioreactor was harvested at time points 18, 21, 24, 27, 30, and 36 hours post infection (hpi). Cells and debris were removed by centrifugation (800 × g, 10 min, 4 °C) and the supernatant (“virus harvest”) was clarified by 0.45 µm filtration (Minisart, SFCA, #16555, Sartorius Stedim Biotech; Göttingen, Germany) (“clarified virus harvest”). An enzymatic DNA digestion was made with an unspecific nuclease by supplementing the clarified virus harvest with magnesium chloride (#M8266-1KG; Sigma-Aldrich Chemie GmbH; Munich, Germany) to a final concentration of 2 mM and 10 U/mL Denarase® (named "Denarase" hereafter, #2DN100KU99; Sartorius Stedim Biotech; Göttingen, Germany). The sample was incubated under mixing for 24 h at 37 ºC. The clarified virus harvest was chemically inactivated either before or after the DNA digestion using beta-propiolactone (BPL, #33672.01; Serva Electrophoresis; Heidelberg, Germany) added to a final concentration of 6 mM and incubated at 37 ºC for 24 h. The inactivated clarified virus harvest was filtered (Minisart, 0.22 µm, SFCA, #16534, Sartorius Stedim Biotech; Göttingen, Germany) and stored at −80 ºC until further processing.

Chromatographic purification of virus particles

All chromatography experiments were performed with an ÄKTA Pure 25 (GE Healthcare; Uppsala, Sweden) liquid chromatography system. The UV absorbance was monitored at 280 nm and virus particles were monitored with a NICOMPTM 380 (Particle Sizing Systems; Santa Barbara, USA) submicron particle analyzer at 632.8 nm. All chromatography experiments were performed at room temperature.

Virus capture was done with membrane-based SXC as previously reported (Marichal-Gallardo et al., 2017). Inactivated clarified virus harvests were conditioned prior to SXC to a final concentration of 8 % PEG-6000 (#81260-5KG; Sigma-Aldrich Chemie GmbH; Munich, Germany) using a 32 % PEG-6000 stock solution. The SXC column comprised a stack of 1.0 µm regenerated cellulose membranes (#10410014; GE Healthcare; Uppsala, Sweden) (20 layers; 100 cm^2 total surface) fitted into commercial 25 mm stainless steel filter housings as described before. The flow rate used was 10–15 mL/min. The SXC purifications were performed in bind-elute mode. Briefly, (A) Equilibration: the column was washed with 10 column volumes (CV) of water followed by 10 CV of "SXC equilibration buffer" (50 mM Tris-HCl, 150 mM sodium chloride, 8 % PEG-6000, pH 7.4). (B) Sample injection: the sample was then loaded onto the column followed by a wash step with equilibration buffer until baseline UV absorbance was achieved. (C) Elution: virus particles were recovered by washing with up to 25 CV of Tris buffer (50 mM Tris-HCl, 150 mM sodium chloride, pH 7.4).

The SXC elution pools were subsequently purified by pseudo-affinity chromatography using a SCMA as previously reported (A. R. Fortuna et al., 2018). Commercial sulfated cellulose membranes (94SC--04-001#; Sartorius Stedim Biotech; Göttingen, Germany) were fitted into the same filter housings used for SXC as described above (10 layers; 50 cm^2 total surface). The flow rates used were 10–15 mL/min. The polishing of SXC-purified influenza virions with SCMA was equally carried out in bind-elute. Briefly, (A) Equilibration: the column was

washed with 10 CV of water followed by 10 CV of "SCMA equilibration buffer" (10 mM Tris-HCl, 4 mS/cm, pH 7.4). (B) Sample injection: the sample was then loaded onto the column followed by a wash step with equilibration buffer until baseline UV absorbance was achieved. (C) Elution: virus particles were recovered by washing with 20 CV of "SCMA elution buffer" (10 mM Tris-HCl, 1.0 M NaCl, pH 7.4). Elution fractions from either the SXC or SCMA purification steps were optionally dialyzed with 300 kDa molecular weight cut-off (MWCO) membranes as described previously (Marichal-Gallardo et al., 2017). Dialyzed samples were spiked with sucrose at a final concentration of 1 % before freezing at −80 ºC. Additionally, size exclusion chromatography experiments were carried out with a packed-bead Superdex 200 Increase 10/300 GL column (#17517501; GE Healthcare; Uppsala, Sweden). The sample injection volumes ranged from 50–500 µL and the flow rate was 0.75 mL/min.

Sample preparation

The cell suspension was centrifuged at 800 × g for 10 min at room temperature to remove cells and cell debris. The cell-free supernatant was aliquoted and stored at −80 °C until respective analysis. For quantitation of metabolites, virus containing samples were thawed and inactivated in a heat block at 80 °C for 2 min prior to analysis.

Quantitation of extracellular metabolites and osmolality

Concentration of glucose, glutamate, lactate and ammonium were measured using a BioProfile 100 Plus analyzer (Nova Biomedical, Waltham, USA) using three external standards each. Glutamine was quantified with a Glutamine V2 Bio kit (#07395655001, Roche Diagnostics, Mannheim, Germany) using a Cedex Bio Analyzer (#06395554001, Roche Diagnostics, Mannheim, Germany). Amino acid concentrations were determined with the “UPLC Amino Acid Analysis Solution” using an ACQUITY UPLC H-Class (#720003294en, Waters, Milford, USA). Medium osmolality was measured off-line with a vapor pressure osmometer (VAPRO® 5520, Wescor, Logan, USA).

Infectious virus titer by $TCID_{50}$ assay

For the quantification of infectious IAV particles a $TCID_{50}$ assay was used as described by Genzel and Reichl (Genzel & Reichl, 2007). Cell-free, sterile supernatant was stored until measurement at −80 °C. Confluent adherent MDCK cells (#84121903, ECACC, Public Health, Salisbury, England, UK) cultivated in 96-well plates (GMEM medium) were infected with a serial dilution of virus samples (100 µL) and incubated for 48 h (37 °C, 5 % CO_2). MDCK cells were fixed with an ice-cold acetone solution (80 %), stained with an anti-influenza A/PR/8/34 H1N1 HA serum (#03/242, NIBSC, Ridge, UK) and an Alexa Fluor donkey anti-sheep IgG antibody (#A11015, Thermo Fisher Scientific, Waltham, USA) as a secondary fluorescence label. Fluorescence positive and negative wells were counted using a fluorescence microscope (Axio Observer A1, Zeiss, Oberkochen, Germany) and infectious titer was calculated from eight replicates with the Spearman-Karber method (Kärber, 1931; Spearman, 1909). The infectious virus titer is expressed as $TCID_{50}$/mL.

Virus titer by hemagglutination activity assay

Total influenza virus content was estimated by a hemagglutination activity (aHA) assay as described previously (Kalbfuss, Knöchlein, Kröber, & Reichl, 2008). Virus samples and standards were serially diluted in two dilution rows ($2^{(1-n)}$ and $2^{(0.5-n)}$ with n: 1 to 12) with PBS in 96-round-bottom-wells. A volume of 100 µL of chicken erythrocyte solution was added (2×10^7 erythrocytes/mL) to diluted samples (100 µL) and incubated for 3–8 h at room temperature. The aHA was evaluated using a plate reader (Infinite® M200 microplate reader, Tecan Group, Männedorf, Switzerland) measuring the extinction at 700 nm and the final titer was calculated by a curve fitting function of the resulting extinction data. The aHA titer is expressed as common logarithm (log_{10}) of the hemagglutinination units (HAU) per analysis volume (100 µL): log_{10}(HAU/100 µL). For mass balancing in DSP and further calculations, the HA titer is also expressed in its linear form as hemagglutinination units (HAU) per analysis

volume (100 µL): HAU/100 µL. From this, the corresponding total concentration of virus particles was estimated as follows:

$$\frac{Virus_{total}}{mL} = 2\mathrm{E}7\,\frac{1}{mL}\cdot HAU = 2\mathrm{E}7\,\frac{1}{mL}\cdot 10^{\log_{10}(HAU/100\,\mu L)} \qquad \text{Equation 1}$$

Virus antigen quantitation by single-radial immunodiffusion assay

The amount of the viral hemagglutinin (HA) surface antigen was quantified by a single-radial immunodiffusion (SRID) assay as previously reported (Wood, Schild, Newman, & Seagroatt, 1977). Samples were dialyzed as described before (Marichal-Gallardo et al., 2017) and lyophilized using 1 % sucrose as cryo-protectant. Resuspension was made by adjusting the HA content of the samples to the HA content of a reference standard produced in-house as described by Opitz et al. (Opitz et al., 2009). The assay setups consisted of a 7 × 7 diffusion matrix made of a 1 % agarose gel with 64 µg/mL anti A/PR/8 antigen (#03/242; NIBSC; Hertfordshire, UK). Values are reported in μg_{HA}/mL.

Imaging flow cytometry

The relative amount of infected and apoptotic cells was determined by imaging flow cytometry, as described previously (Frensing et al., 2016). For cell fixation, 1 mL of infected MDCK cells were mixed with paraformaldehyde to a final concentration of 2 % and incubated at 4 °C for 30 min. Cells were washed with PBS (300 × g, 10 min, 4 °C), added to 5 mL cold (−20 °C) 70 % ethanol and stored at −20 °C. For staining, fixed cells in ethanol were spun down (300 × g, 10 min, 4 °C) to remove storage solution. The cell pellet was washed twice with FACS-buffer (PBS containing 0.1 % BSA and 2 % glycine) and blocked in PBS containing 1 % BSA (30 min, 37 °C). vRNP positive cells were stained with a monoclonal mouse anti-NP antibody mAb61A5 (Momose, Kikuchi, Komase, & Morikawa, 2007) as a primary antibody, and Alexa Fluor 647-conjugated goat anti-mouse pAb (#A21235, Thermo Fisher Scientific, Waltham, USA,) as a secondary antibody. All antibodies were incubated for

60 min at 37 °C in FACS-buffer. Between each incubation step, cells were washed twice with FACS-buffer (300 × g, 10 min, 4 °C). Shortly before the analysis, nucleic DNA was stained with DAPI. Ten thousand single cells were analyzed with an ImageStream X Mark II (#100220, Merck, Darmstadt, Germany) using a 60× objective lens. Image analysis was carried out with the IDEAS software (version 6.1). The vRNP-positive cells were considered as infected and nucleic condensation and fragmentation were considered a sign of apoptosis.

Quantitation of total protein and host cell DNA

Total protein was estimated using a Bradford BioRad assay (#5000006; BioRad Labo ratories; Hercules, USA). The calibration curve was made with bovine serum albumin (BSA) (#A3912; Sigma-Aldrich Chemie GmbH; Munich, Germany) in the range of 5–40 µg/mL with a limit of detection (LOD) of 0.4 µg/mL. The concentration of dsDNA was estimated with a Quant-iT™ PicoGreen assay (#P7581; Life Technologies GmbH; Darmstadt, Germany). The standard curve was made with lambda DNA (# D1501; Promega; Madison, USA) for the range of 4–250 ng/mL with LOD of 1.6 ng/mL. This assay is referred as "PicoGreen" hereafter.

Particle size distribution by differential centrifugal sedimentation

Differential centrifugal sedimentation (DCS) analysis was performed using a CPS DC24000 UHR disc centrifuge (CPS Instruments Inc.; Los Angeles, USA) at 24,000 rpm with a 4–16 % (m/v) sucrose gradient in 50 mM Tris, 150 mM NaCl, pH 7.4 buffer, as reported previously (Pieler, Heyse, Wolff, & Reichl, 2017). Briefly, the gradient consisted of nine 1.6 mL steps with different sucrose concentrations each, i.e. 16 %, 14.5 %, 13 %, 11.5 %, 10 %, 8.5 %, 7 %, 5.5 %, and 4 % sucrose (m/v), with a total volume of 14.4 mL. The gradient quality was evaluated by injecting a 239 nm particle standard (0.3–0.5 % solid content, polyvinyl chloride, CPS Instruments Inc.; Los Angeles, USA) directly after gradient injection. Then, the gradient was equilibrated for 10 min, followed by another 239 nm particle standard injection for

measurement calibration. Finally, 100 µL of sample (1:1) were injected for the size distribution measurements of chromatography elution fractions. Additional density parameters for solutions and particles introduced into the software were 1.072 g/mL for the gradient buffer, 1.385 g/mL for the calibration particles, and 1.180 g/mL for influenza A virus. The particle size distributions are displayed as normalized weight average in percentage against apparent hydrodynamic diameter in nm.

Transmission electron microscopy

Transmission electron microscopy (TEM) of virus particles was done by negative staining. A solution containing virions was applied to glow-discharged carbon coated 400 mesh copper grids, and stained with 1 % uranyl acetate. Virions were adsorbed to a continuous carbon film, attached to a Quantifoil (3.5/1) (Quantifoil, Jena, Germany) grid and freeze-plunged in a Leica EM GP (Leica, Wetzlar, Germany) employing the blotting sensor at 75 % humidity and −24 ºC. Images were taken in a Philips CM120 electron microscope (Philips Inc.) using a TemCam F416 CMOS camera (TVIPS, Gauting, Germany).

Results

Optimization of stirred tank bioreactor cultivations

In preliminary studies, various cultivation conditions and infection parameters were evaluated for the cell growth and virus production phase in shake flasks and stirred tank bioreactors (STR). In particular, different agitation speeds from 80 rpm to 140 rpm were tested for suspension MDCK cultivation in the DASGIP system. Based on results obtained for cell growth, a stirring speed of 80 rpm was selected for subsequent process evaluations (data not shown). The pH control set points for the cell growth phase and the virus infection phase were 7.00 and 7.20, respectively. Furthermore, based on scouting experiments in shake flasks, an MOI of 10^{-3} and a final trypsin concentration of 30 U/mL were used. For process evaluation, cell growth dynamics, viable cell concentration and cell volume, viability, and virus yields were monitored in three parallel stirred tank bioreactors (STR1–3).

Cell growth phase

With the used cultivation conditions, excellent growth of the MDCK suspension cell line adapted to Xeno-CDM was observed. After a short lag phase, cells grew exponentially within three days to a concentration of 9.5±0.5 × 10^6 cells/mL (Fig. 1 A). While cell diameters and cell concentrations showed some slight variations between batches after inoculation and in the last 24 h of the cell growth phase (Fig. 1 A&D), the viable cell volume was rather consistent between batches (Fig. 1 B). The average maximal value was 14.7±0.5 µl/mL. Based on the viable cell volume, uptake and release rates for the main metabolites were determined as shown in the supplementary (Fig. S2).

Fitting of exponential growth functions to cell concentrations and cell volumes (Fig. 1 B) resulted in an average specific growth rate of µ=0.033 h^{-1} (8–72 1/h) and µ=0.031 1/h (0–72 h) for cell concentrations and cell volumes, respectively. Over the whole cell growth phase cell viability was consistently high (>97 %) and even increased slightly towards the end of the growth phase (> 98 %). Neither for the main extracellular metabolites (Figure 2 A&B) nor the

majority of amino acids (Figure 3 & Figure S3) any obvious limitation was found. Only the amino acids leucine, isoleucine, and methionine were below the limit of quantification at the end of the growth phase (Figure 3 D–F). Cultivation and infections performed with higher initial leucine, isoleucine, and methionine concentrations neither increased cell concentration nor virus titer (data not shown). Accumulation of the by-products lactate and ammonium (Figure 2 C&D) was expected but concentrations remained in a reasonable range where negative effects on metabolism or cell growth most likely do not play a significant role (M. Gagnon et al., 2011; Schneider, Marison, & von Stockar, 1996; Slivac, Blajić, Radošević, Kniewald, & Gaurina Srček, 2010). In addition to lactate and ammonium, the amino acids glutamate, alanine and – to a lesser extent – aspartate were produced (Figure 3 A–C), presumably as by-products of the cellular transamination in glutamine metabolism (Eagle, 1959; Schneider et al., 1996).

Infection phase

For infection, cells were diluted by half to approximately 5×10^6 cells/mL by adding fresh medium containing IAV for a final MOI of 10^{-3}. Trypsin activity was adjusted to 30 U/mL. MDCK cells continued to grow after infection reaching a maximal viable cell concentration of approximately 7×10^6 cells/mL at 21 hpi (Figure 1A) (Figure 1A). Afterwards, the cell concentration started to decrease. Cell viability initially increased slightly (99 %) but also started to decrease with the onset of virus accumulation (>21 hpi) (Figure 1C). Similarly, cell diameters decreased significantly during virus production (Figure 1D), due to virus-induced apoptosis and cell lysis. In contrast to the reduction in cell size during the growth phase (reduced osmolality), medium osmolality increased due to lactate release (Figure 2C) and base addition for pH control (Figure S1A). With the medium addition and the increase in working volume at time of infection, cellular nutrients were replenished and by-products diluted. Similar to the growth phase, no significant limitation of main metabolites (Figure 2) and most analyzed amino acids (Figure 3 & S3) were found in the infection phase. As for the growth phase, isoleucine and methionine were below the limit of quantification (>18 hpi). As expected, uptake and release rates of main metabolites and by-products increased

significantly immediately after addition of fresh medium (Figure S2). Later, the rate of glucose uptake and lactate release decreased while the rates for glutamine and ammonium remained rather constant (until about 15 hpi). With full infection of the cell population at 15–18 hpi (Figure 4C) cells consumed more glucose and produced more lactate, but glutamine consumption and ammonium production declined rapidly (Figure S2). Lactate continued to accumulate and exceeded 40 mM at the end of infection phase.

Combining image stream analysis and virus quantification assays enabled to follow the virus replication dynamics. Fast virus replication led to an early increase in $TCID_{50}$ values and the percentage of infected cells, with a maximum at 18–27 hpi and 15–18 hpi, respectively (Figure 4B&C). A maximal infectious virus titer of $2.7\pm0.5 \times 10^9$ $TCID_{50}$/mL (21 hpi) was measured, followed by a titer reduction due to degradation of infectious virus particles (>27 hpi). A significant accumulation of aHA was not detected until 12 hpi, at which point it increased rapidly and plateaued (27 hpi) at 3.66 ± 0.06 $\log_{10}$(HAU/100 µL) (Figure 4A). With the infection spreading over the entire cell population, the percentage of apoptotic cells started to increase 12 hpi and reached a maximum (approx. 80 %) at the end of the infection phase (Figure 4D).

Identification of the optimal harvest point

Manufacturing processes for biopharmaceuticals require an adequate integration of USP and DSP operations in order to reduce process time and costs. In addition, it is advantageous to minimize the contamination level for subsequent purification steps. Following the increase in virus titers we observed a significant increase in the total protein and DNA concentration of the cell-free supernatant. While the total protein concentration increased only about fivefold, the DNA level increased by two orders of magnitude compared to the DNA concentration measured in the cell growth phase (Figure 5 A&C). Total protein concentration started to increase already during the cell growth phase and increased rapidly at a later time of infection due to virus release (viral proteins) and virus-induced cell death (host cell proteins) (Figure 5 A). In contrast, the level of host cell DNA remained more or less stable (100 ng/mL)

during the cell growth phase, but increased strongly after trypsin addition (time of infection). Most likely, the addition of trypsin led to the lysis of “dead” cells resulting in a slight increase in cellular viability (>99 %) and the release of cellular DNA. At a later stage of infection, very high levels of DNA (> 2 µg/mL) were measured due to extensive virus-induced apoptosis and cell death (Figure 5 C).

To identify the optimal time point for virus harvesting, the ratio of virus product (using linear HAU values) to the total protein and the ratio of virus product to the host cell DNA concentration were determined (Figure 5 B&D). For all STR replicates, maximum ratios were found at 21–24 hpi with 80–100 HAU/(μg_{prot}/mL) and 3–4 HAU/(ng_{DNA}/mL), respectively (Figure 5, B & D). For both time points, the aHA titer (3.60±0.06 $\log_{10}$(HAU/100 µL)) almost reached its plateau, but the ratio of virus product to the corresponding impurity decreased rapidly starting 24 hpi. It cannot be excluded that the further increase in aHA value (>24 hpi) does not reflect the release of virions but the accumulation of HA containing cell debris. This is also supported by the fact that cell viability remained stable at >95 % from the time of infection up to 24 hpi, after which it dropped significantly (Figure 1). The clarified virus harvests from 21 and 24 hpi were pooled for DSP experiments and analytics.

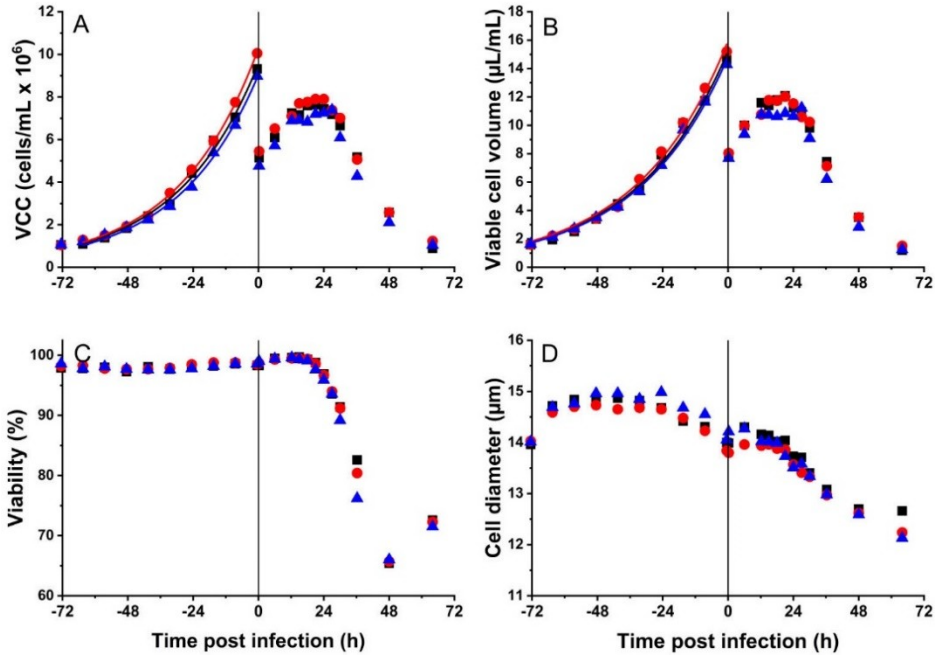

Fig. 1 MDCK suspension cells cultivated in three parallel bioreactors for IAV production. Viable cell concentration (A), viable cell volume (B), viability (C) and average cell diameter (D) were monitored over the whole process time (144 h). Cell concentrations (A) and cell volumes (B) were fitted to an exponential growth function (curves) to determine the specific growth rate. Vertical lines indicate time of infection, where cell suspension was diluted by half. STR1 (■), STR2 (●), STR3 (▲)

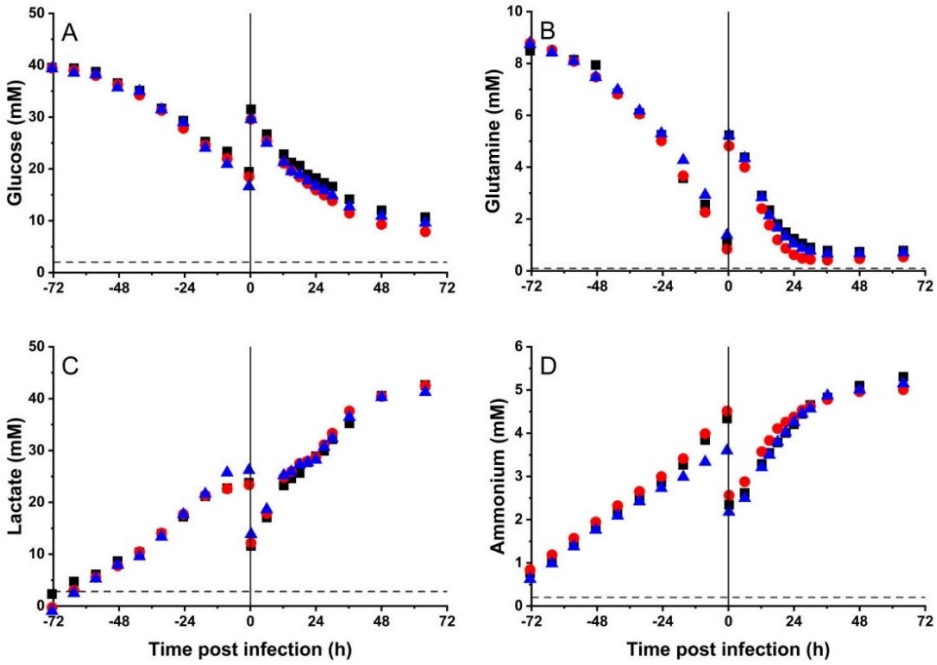

Fig. 2 Main extracellular metabolites in three parallel bioreactors for IAV production. Concentration of the main metabolites glucose (A), glutamine (B), lactate (C) and ammonium (D) in the cell culture medium over the process time (144 h). Vertical lines indicate time point of infection. Horizontal dashed lines indicate limit of quantification of the respective metabolite. STR1 (■), STR2 (●), STR3 (▲)

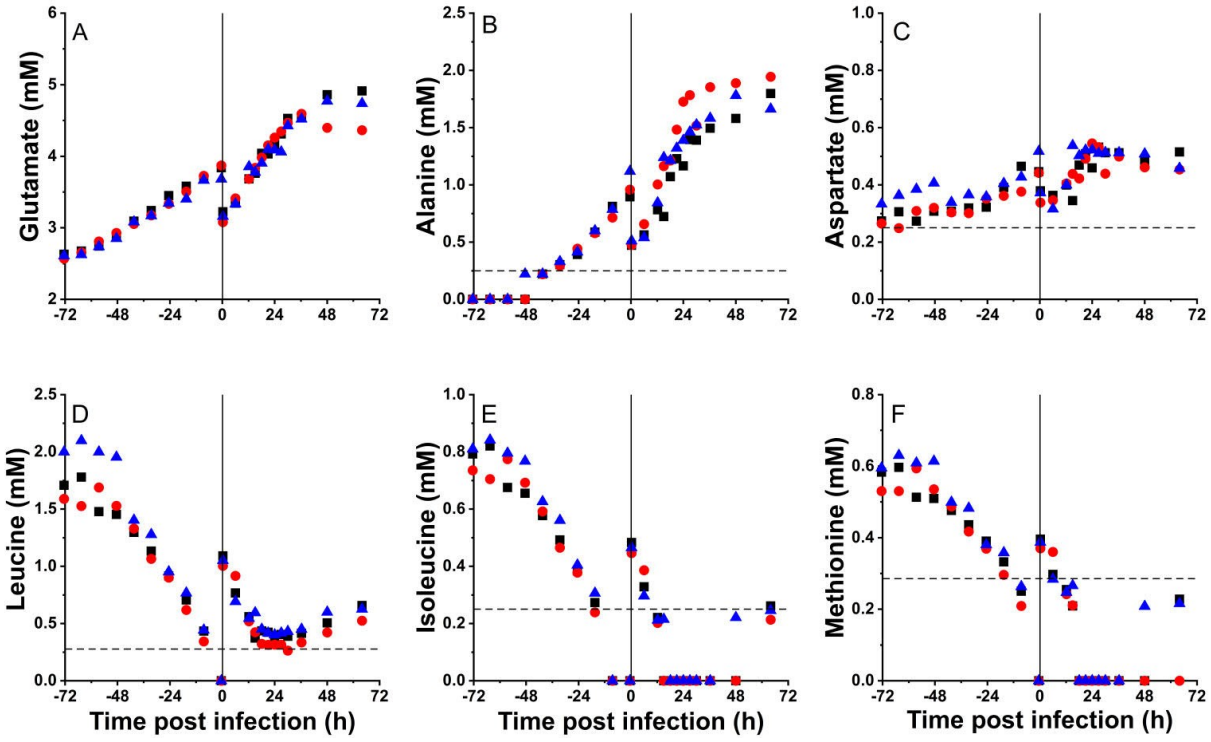

Fig. 3 Concentration of selected amino acids in three parallel bioreactors for IAV production. Extracellular concentration of the amino acids glutamate (A), alanine (B), aspartate (C), leucine (D), isoleucine (E) and methionine (F) in the cell culture medium over the process time (144 h). Vertical lines indicate time point of infection. Horizontal dashed lines indicate limit of quantification of the respective amino acid. STR1 (■), STR2 (●), STR3 (▲)

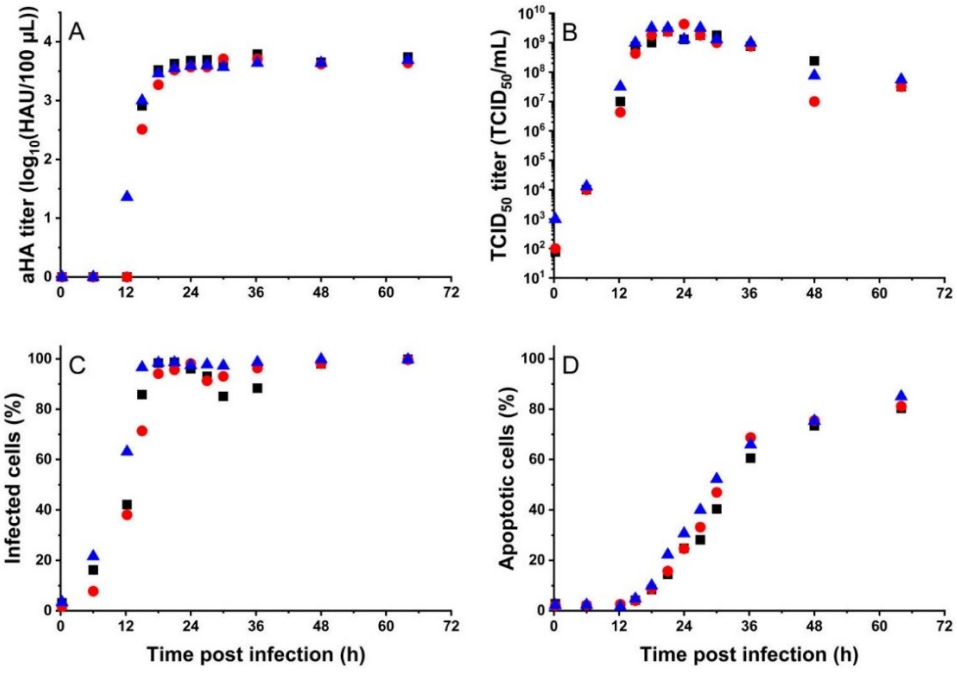

Fig. 4 Virus titers and cell infection dynamics in three parallel bioreactors for IAV production. Total virus titer based on hemagglutination activity (A), infectious virus titer based on $TCID_{50}$ assay (B), percentage of infected (C) and apoptotic (D) MDCK cells. STR1 (■), STR2 (●), STR3 (▲)

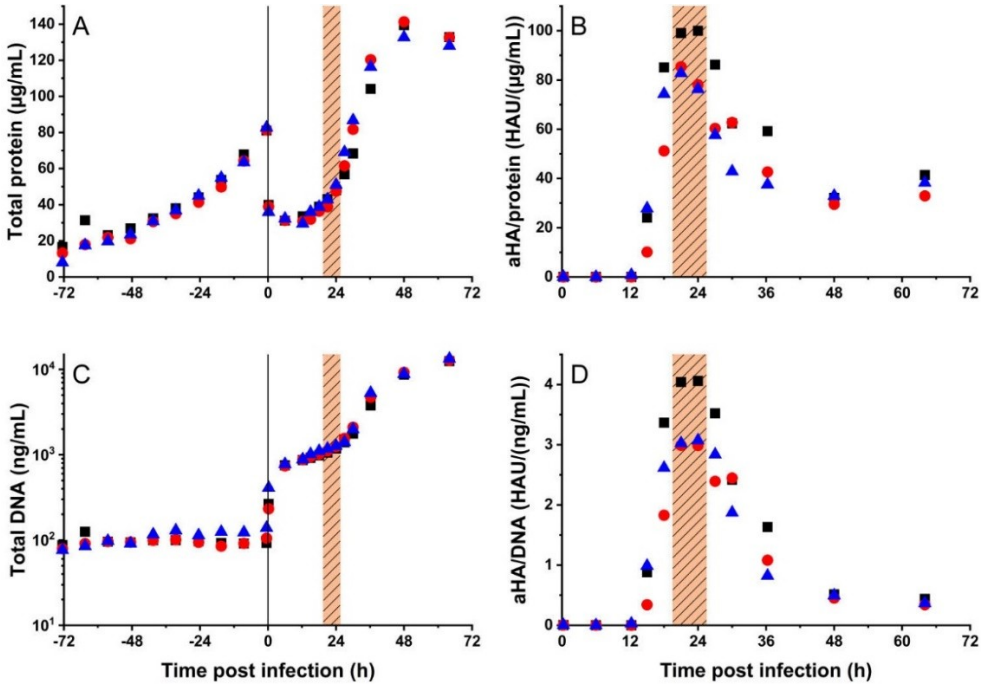

476

477 **Fig. 5 Total protein and host cell DNA profiles in three parallel bioreactors for IAV production.**
478 Total protein (A) and total DNA (C) concentrations during the cultivation process. The ratio of total
479 protein (B) and DNA (D) to the virus titer (aHA assay) was used to identify the optimal virus harvest
480 point (shaded area). Vertical lines indicate time point of infection. STR1 (■), STR2 (●), STR3 (▲)

481

482

Influenza A virus harvest, DNA digestion and chemical inactivation

Low speed centrifugation (800 × g) followed by dead-end microfiltration (0.45 µm) were used to remove cells and cell debris. For the pooled harvests of the optimal time of harvest (21/24 hpi) minimal amount of cell debris after centrifugation eased subsequent filtration step (no membrane blockage). No significant losses of aHA titers were observed for the clarified harvest material (Table 1). The DNA concentration of the clarified virus harvest was 1.2 µg/mL (Table 1). The DNA levels in the supernatant were lower when the DNA digestion was performed before the chemical inactivation by BPL (see supplementary data). The host cell DNA and protein concentrations in the digested, inactivated clarified virus harvest were around 28 ng/mL and 30 µg/mL, respectively (Table 1).

Chromatographic purification of virus particles

A representative chromatogram of SXC purification step is shown in Figure 6A. Impurities such as host cell DNA and proteins were washed away in the flow-through and monitored by UV absorbance. The IAV particles were traced by light scattering, with a nil signal in the flow-through and a clear peak during elution. There was no aHA titer detected in the flow-through (Table 1), confirming the light scattering signal monitored during the chromatography run. Offline analysis of the eluate showed that the virus yield for the SXC was 115.2 %±10.2 and 108.0 % according to the aHA and SRID assays, respectively. The SXC eluate contained 58.4 %±0.4 of the total protein and 20.6 %±2.2 of the DNA loaded (Table 1). The eluate volume was 25 mL and was concentrated around threefold relative to the load (73.6 mL). After SXC, a pseudo-affinity chromatography polishing step was performed using a SCMA. Similar to IEX, SCMA chromatography requires low conductivity for product loading. Therefore, the SXC eluate was diluted around fourfold with SCMA binding buffer to a conductivity of 4 mS/cm. As shown in the SCMA chromatogram in Figure 6B, the UV and light-scattering signals in the flow-through were practically nil, suggesting the high purity of the loaded product and the capture of virus particles. After a washing step, the IAV particles

were eluted with a high salt buffer. The product yield in the SCMA eluate was 83.6 %±15.5 and 56.0 % according to the aHA and SRID assay, respectively. The eluate contained 49.3 %±0.4 of the total protein and 43.6 %±5.5 of the DNA loaded (Table 1) and was concentrated around tenfold (8.9 mL) relative to the load (104.6 mL).

The purified SXC eluate showed a single peak in SEC at the retention time of around 7.5 mL with no notable impurities, compared to the SEC fingerprints of the inactivated clarified virus harvest before purification (Figure 7A). TEM pictures of the purified virus (inset) showed particles with spherical shape and a size of 80–100 nm. Purity was also confirmed by size distribution analysis of the virus particles by DCS (Figure 7B) in comparison to a process established previously (Marichal-Gallardo et al., 2017). Both the inactivated virus harvest and the purified virus samples from this work showed a monodisperse peak at around 80 nm with a few virus dimers that were slightly more notable in the purified product. Compared to the particle size distributions of the previous process, far less submicron-sized particles are observed (Figure 7B). This was probably due to the earlier harvest time of 21–24 hpi chosen for this process, compared to 72 hpi used previously (Marichal-Gallardo et al., 2017).

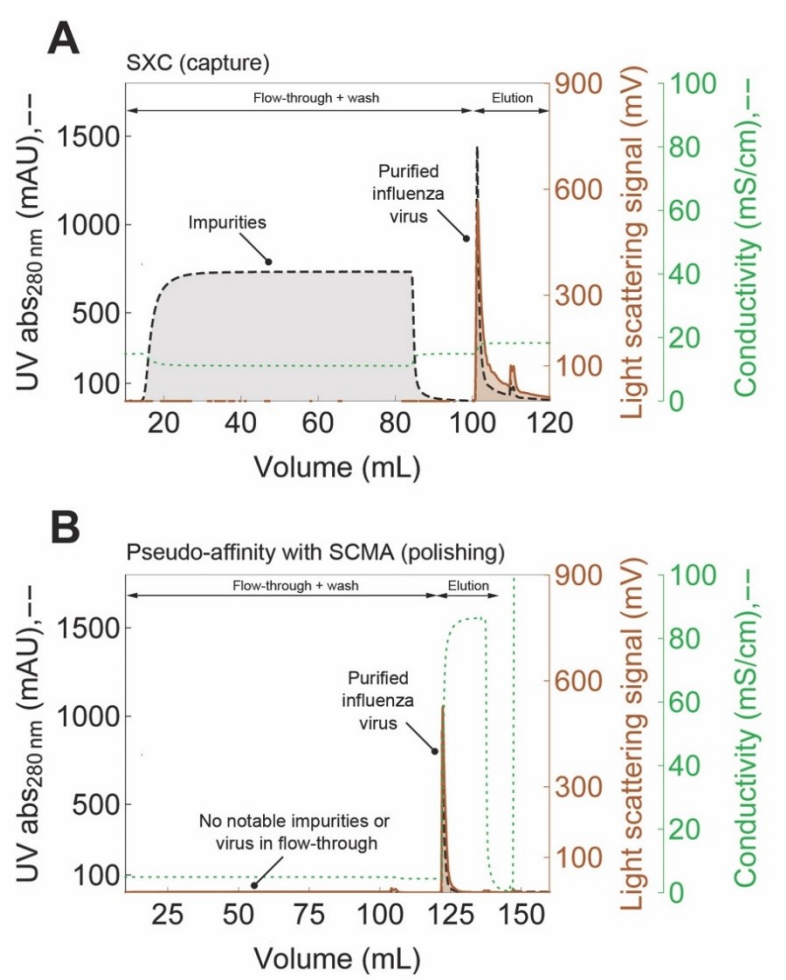

Fig. 6 Chromatographic purification of IAV particles produced in 1 L STRs. Virus capture by SXC (A) using a column packed with regenerated cellulose membranes (100 cm^2). After SXC, a polishing step was performed by pseudo affinity chromatography with a SCMA of 50 cm^2 (B). Virus particles were traced online by light scattering and total protein by UV absorbance. For mass balances and percentage yields refer to Table 1.

Table 1 Mass balances and percentage yields from the chromatographic purification of influenza A virus particles produced in 1 L STRs by capture with SXC and pseudo-affinity chromatography for polishing with a SCMA.; mean ± standard deviation of the mean of analytical triplicates.

		Virus product						Impurities					
	Vol.	aHA[a]			HA antigen[b]		Total protein[c]			host cell DNA[d]			
Step	(mL)	HAU/100 µL		%	µg/mL	%	µg/mL		%	ng/mL		%	
Harvest (21+24 hpi)[e]		3,896.1 ± 104.6		n.d.	n.d.		45.2 ± 3.6		n.d.	1,171.2 ± 58.6		n.d.	
Clarification (0.45 µm)		3,536.4 ± 141.2		n.d.	n.d.		38.9 ± 1.2		n.d.	974.1 ± 11.8		n.d.	
Digestion + inactivation[f]	50.0	1,576.5 ± 105.3		n.d.	4.4		29.5 ± 2.9		n.d.	27.8 ± 2.2		n.d.	
SXC load	73.6	1,070.8 ± 71.6	100.0		2.9	100.0	22.7 ± 0.1	100.0		12.7 ± 0.7	100.0		
SXC elution	25.0	3,633.5 ± 209.9	115.2 ±	10.2	9.3	108.0	39.1 ± 0.1	58.4 ±	0.4	7.7 ± 0.7	20.6 ±	2.2	
SCMA load	104.6	568.5 ± 104.6	100.0		1.8	100.0	7.8 ± 0.0	100.0		1.5 ± 0.1	100.0		
SCMA elution	8.9	5,584.4 ± 115.4	83.6 ±	15.5	11.8	56.0	45.3 ± 0.3	49.3 ±	0.4	7.9 ± 0.7	43.6 ±	5.5	

HAU=hemagglutination units; hpi=hours post infection;
[a] by hemagglutination activity (aHA) assay
[b] by single radial immunodiffusion (SRID) assay
[c] total protein by Bradford assay
[d] dsDNA by PicoGreen assay
[e] centrifuged at 800×g
[f] enzymatic DNA digestion followed by chemical inactivation with ß-propiolactone

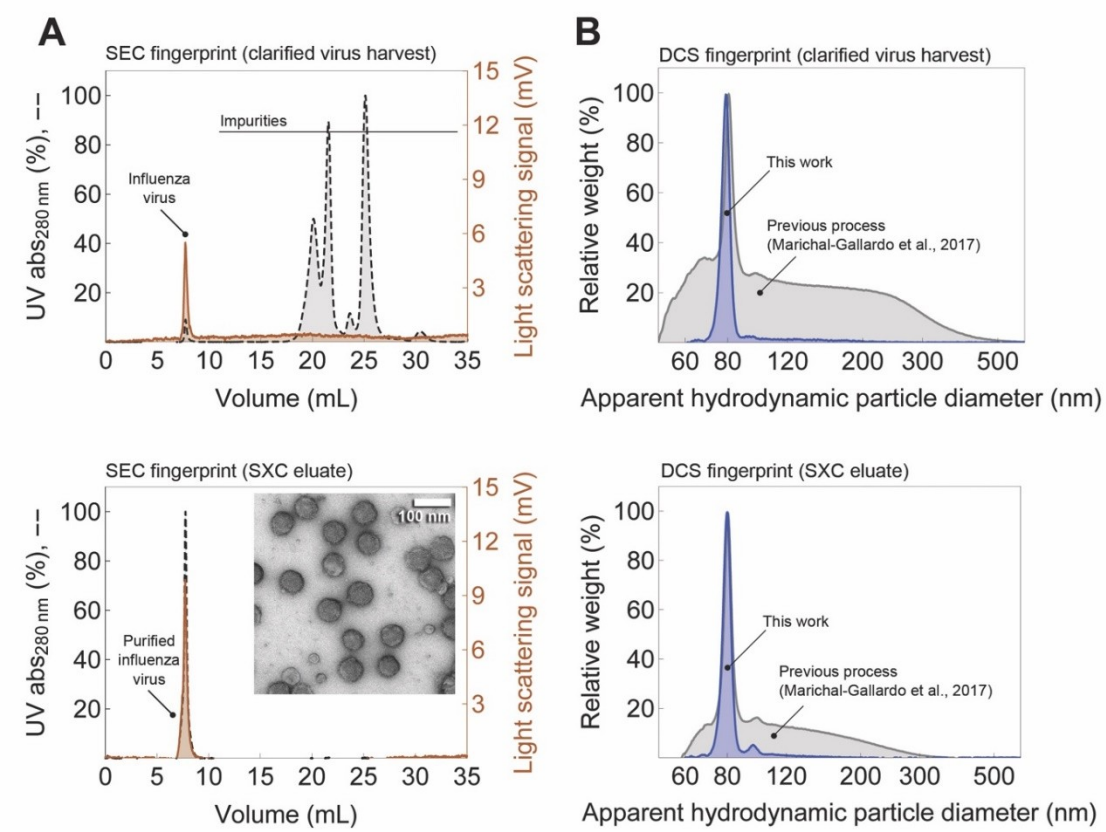

537

538 **Fig. 7 SEC fingerprints and DCS fingerprints of inactivated and clarified IAV harvests and SXC**
539 **eluates.** (A) The inset in the lower panel is a TEM picture of the purified virus particles. (B) For
540 comparison of particle size distributions by DCS, samples from this work (blue curves) are shown in an
541 overlay with samples from a similar process described previously (gray curves).

542

Discussion

Cell growth and metabolism

For high yield cell culture-based vaccine manufacturing processes, high specific cell growth rates, viability and cell concentrations are fundamental. Neglecting any of these aspects will result in compromises regarding productivity, scalability, robustness and costs of a large-scale manufacturing process. This was also highlighted for MDCK suspension cell-based processes reported previously (Castro et al., 2015; Chu et al., 2009; Lohr et al., 2010; van Wielink et al., 2011). With a MDCK cell line exceeding 10×10^6 cells/mL that grows as single cell suspension in a chemically defined medium with a doubling time of 21 h at a viability over 97 % in STR systems, a big step towards a highly competitive process is taken. Additionally, growth performance of MDCK cells cultivated in Xeno-CDM medium was very reproducible, which eases scale up and reduces batch-to-batch variations in USP. The established process strategy not only displayed an excellent growth performance of the cell line, but also demonstrated optimal utilization of substrates and amino acids. Whereas glucose was available in access over the whole process, glutamine and other amino acids were almost depleted towards the end of the cultivation phase and were restored partly by the fresh medium feed at time of infection. Despite a relatively strong lactate accumulation (maximal 42 mM) there was no or only a minor impact on pH and medium osmolality. A high initial glutamine concentration (>8 mM) and high specific consumption rates (30–40 fmol/(h cell)) led to ammonium concentrations of 4–5 mM both for cell growth and infection phase. For process intensification, the use of a feeding strategy using an adapted medium formulation could help to avoid volume expansion and allow to increase virus titers while reducing lactate and ammonium accumulation (M. Gagnon et al., 2011; Ljunggren & Häggström, 1994; Maranga & Goochee, 2006). Alternatively, glutamine and glucose could be replaced with substrates that can reduce the production of by-products (Altamirano, Paredes, Cairó, & Gòdia, 2000; Christie & Butler, 1999; Freund & Croughan, 2018; Genzel, Ritter, König, Alt, & Reichl, 2005). Nevertheless, in the established process we see no clear

indication for inhibition of cell growth or virus replication due to lactate or ammonium accumulation.

Influenza virus production

With the application of a new cultivation medium designed for MDCK suspension cells, very high IAV titers were achieved. High cell concentrations, combined with high cell specific productivity (>11,000 total virions/cell; 300 $TCID_{50}$/cell) allowed to reach IAV titers that are among the highest reported for batch- or extended batch processes, and the highest titers obtained in STR systems with chemically defined media (Bissinger et al., 2019; Bock et al., 2011; Hu et al., 2011; D. Huang et al., 2015; Le Ru et al., 2010; Peschel, Frentzel, Laske, Genzel, & Reichl, 2013). Furthermore, high cell growth and fast virus replication reduced the USP production time from 7 to 4 days, compared to adherent MDCK cells (Genzel, Fischer, et al., 2006; Genzel, Olmer, Schäfer, & Reichl, 2006; Hu et al., 2008). In combination with the achieved virus titers (3.6 $\log_{10}$(HAU/100 µL) & >2 × 10^9 $TCID_{50}$/mL) this increases overall productivity, and can support fast manufacturing of pandemic vaccines.

Transition from USP to DSP

One of the most important aspects regarding process intensification in USP is the control of protein and host cell DNA contamination levels in the DSP train. Challenges arise if the time point of harvest is not selected properly and IAV-induced cell lysis results in an unnecessary high release of contaminants. As a consequence, it might be required to increase the number of DSP unit operations with a negative impact on process yield and cost effectiveness. For instance, the clearance of cellular chromatin — one of the most persistent process impurities — is challenging even for affinity-based purification methods. Therefore, it is desirable to harvest the product in a time window where titers peak but cell lysis is not too advanced (P. Gagnon et al., 2014; P. Gagnon, Nian, Yang, Yang, & Lim, 2015; Nian & Gagnon, 2016; Tan, Yeo, Yang, & Gagnon, 2015). Here, we identified the optimal harvest point based on the highest ratio of virus titer to total protein (Figure 5B) and host cell DNA (Figure 5D) in order to minimize the amount of impurities for subsequent DSP steps. For each of the three STRs,

the best ratio of virus product to impurities was in a time window of 21–24 hpi and therefore, harvests were pooled for DSP (see Figure 5). The slightly higher product to impurity ratio of STR number 1 compared to STRs number 2 and 3 was most likely attributed to normal batch-to-batch variation.

The placement of the enzymatic DNA digestion step in the process was an additional factor to be considered for reduction of the amount of host cell DNA before the chromatography. Two options were tested: placing the nuclease treatment either before or immediately after the chemical inactivation of IAV with BPL. The DNA concentration was reduced more than threefold by performing the nuclease digestion step before the BPL treatment (Table S1). BPL induced cross-linking reactions between nucleic acid and proteins might explain higher residual DNA in case inactivation is performed first, as the DNase might not be able to digest the chemically-modified DNA (Kubinski and Szbalski, 1975). Depending on the process train, BPL inactivation of the purified product might allow to further reduce the level of host cell DNA as reported previously (Gregersen, Schmitt, Trusheim, & Bröker, 2011).

Virus purification

Membrane-based SXC was used successfully as a capture step with virtually full product yield for both the total IAV content (aHA assay) and the HA concentration (SRID assay) as previously reported for a similar process (Marichal-Gallardo et al., 2017). Compared to other chromatography techniques for purification of IAV, SXC appears to be comparable or better in terms of product recovery and ease of use, as also discussed previously (Marichal-Gallardo et al., 2017). The ability to load and recover the product at physiological salt concentration and pH value minimizes the risk of losing biological activity compared to other techniques. Additionally, different influenza virus strains could be purified using the same process conditions, rendering SXC a promising and efficient platform technology for cell culture-based influenza vaccine manufacturing (data not shown). In this study, most of the host cell DNA was cleared by the nuclease treatment before SXC. The SXC step additionally cleared about 80 % of DNA and about 40 % of total protein. Interestingly, the subsequent

polishing step using a SCMA did not further improve the purity of the virus particles (Table 1), evidencing the importance of carefully selecting the harvesting time point and the order of the unit operations.

Table 2 Estimated number of influenza vaccine doses (15 μg_{HA} per dose) after purification with SXC and SCMA; mean ± standard deviation of the mean of analytical triplicates.

	aHA[a]	HA antigen[b]	Purified doses[c]	Protein per	DNA per
Step	Yield (%)	Yield (%)	per L of harvest	dose (µg)[d]	dose (ng)[e]
SXC	115.2 ± 10.2	108.0	309	63.3 ± 0.2	12.5 ± 1.1
SCMA	83.6 ± 15.5	56.0	173	57.5 ± 0.3	10.0 ± 0.9
Mean	**96.3 ± 1.6**	**60.4**			

[a] by hemagglutination activity (aHA) assay
[b] by single radial immunodiffusion (SRID) assay
[c] monovalent dose of 15 μg_{HA}
[d] total protein by Bradford assay; <6 × HA antigen content & <100 µg per strain total protein per dose
[e] dsDNA by PicoGreen assay; max. 10 ng per dose

Considering a monovalent vaccine dose of 15 μg_{HA} (SRID assay), Table 2 shows that the SXC and SCMA eluates are either below the accepted contamination levels for protein (<100 µg per strain per dose) or close to the maximum of 10 ng of DNA per dose accepted. However, according to Ikeda et al., and based on our experience, the DNA concentrations measured with the PicoGreen assay (as short as 20 bp) are about 5–10 times higher than those detected with the Threshold assay that quantifies fragments larger than 100 bp and is often used for product release (Ikeda, Iwakiri, & Yoshimori, 2009; Marichal-Gallardo et al., 2017; Weigel et al., 2016). Assuming a ratio of five would hypothetically result in a residual DNA contamination level of around 2 ng per monovalent dose. As PicoGreen quantification also detects RNA (with about 100 times lower sensitivity), the actual DNA level in the final product could be even lower (Singer, Jones, Yue, & Haugland, 1997). Eventually, the evaluation of the performance of the process established will depend on the specific assay validated for product release. Either SXC only or a combination of SXC and SCMA seem to be feasible. Both methods can be operated at higher flow rates compared to packed beds using beads and are not impaired by diffusion and performance limitations typically found for large molecule separations. In addition, scale-up of SXC and SCMA is linear by simply increasing the membrane surface, and options are available for single-use operation for both

options allowing fast set up and operation. Here, the combination of both chromatography methods resulted in a product yield of around 96 % by aHA assay and 60 % by SRID assay. This would be equivalent to about 170 doses/L (5.9 mL/dose) of virus harvest. In case only SXC is used, about 300 doses/L (3.3 mL/dose) of virus harvest are to be expected. Regarding overall losses of the entire DSP train, improvements can be made primarily in the initial clarification, inactivation and DNA digestion steps before the SXC capture step (Table 1). Finally, as unit operations proposed yield purified whole virus particles, additional DSP steps might be required for formulation of split or subunit vaccines (Bron, Ortiz, Dijkstra, Stegmann, & Wilschut, 1993; Cusi, 2006).

Integrated process performance

For vaccine production, not only individual process steps but options for scale-up and process integration are crucial. Based on the growth properties of the MDCK suspension cell line developed, we would assume a reduced lead time to reach manufacturing scale (i.e., 2,000 or 10,000 L), compared to other cell lines with a higher cell doubling time and a lower maximal cell density (e.g., t_D 30 h; VCC 5×10^6 cells/mL). Furthermore, the established production process is short and more productive than other processes using MDCK suspension cell lines (D. Huang et al., 2015; Lohr et al., 2010; Wang et al., 2017). Due to high losses of aHA activity (50 %) and viral antigen in the initial DSP steps (DNA digestion and inactivation), a productivity of 300 vaccine doses (15 µg/dose) per liter of cultivation volume was determined. Further optimization are needed in this process steps, for a better evaluation of the true process performance. With the assumption of a fixed aHA to HA protein ratio (400 in this case) an HA antigen content of roughly 9 µg/mL was estimated for the clarified harvest which would correlate to a potential USP production capacity of approximately 600 doses/L. Furthermore, the applied polishing strategy using SCMA improved purity only marginally but with additional product losses. With the application of the designed process the production of three million vaccine doses (15 µg/dose) would be feasible at 10,000 L scale with the potential to obtain up to six million doses (optimized inactivation and DNA digestion).

From small scale purification experiments with the membrane-based chromatography we estimated a productivity as high as 4,600 doses/(m^2 h) (15 µg/dose). Both SXC and SCMA might be operated at industrial scales with devices similar to ones already available for other chromatography techniques (i.e membrane chromatography capsules) with a surface area of 18 m^2 and an estimated capacity to purify about 83,000 doses/h according to our calculations. Concerning the resulting quality of the vaccine candidate we were only able to assess structural integrity and purity. Additional animal trials would be necessary as a next step towards a commercial product. With this the effective vaccine dose can be determined in clinical follow-up studies and additional critical process parameter concerning product quality could be identified.

Overall, we believe that it would be feasible to use the presented process with minor optimization for the fast manufacturing of large quantities of influenza vaccines, thus significantly improving pandemic preparedness. Based on a comprehensive data set of three parallel stirred tank bioreactor runs, a straight forward process development into next scales or even towards a perfusion process at even higher cell concentrations should be straight forward.

Acknowledgements

The authors would like to thank Claudia Best, Nancy Wynserski, Lisa Fichtmüller, and Anja Bastian for their excellent technical support. The authors greatly appreciate the contribution of Shanghai BioEngine Sci-Tech by providing the Xeno-CDM medium.

Funding

YW acknowledges the financial support of the China Scholarship Council. PMG acknowledges the financial support of CONACyT Mexico.

Conflict of Interest

Wen-Song Tan and Xuping Liu are affiliated as directors with Shanghai BioEngine Sci-Tech and were involved in the development of the Xeno-CDM medium both for scientific and commercial purposes. The remaining authors declare that they have no conflict of interest.

References

Aggarwal, K., Jing, F., Maranga, L., & Liu, J. (2011). Bioprocess optimization for cell culture based influenza vaccine production. *Vaccine*, *29*(17), 3320-3328. doi:10.1016/j.vaccine.2011.01.081

Altamirano, C., Paredes, C., Cairó, J. J., & Gòdia, F. (2000). Improvement of CHO Cell Culture Medium Formulation: Simultaneous Substitution of Glucose and Glutamine. *Biotechnol Prog*, *16*(1), 69-75. doi:10.1021/bp990124j

Audsley, J. M., & Tannock, G. A. (2004). The role of cell culture vaccines in the control of the next influenza pandemic. *Expert Opinion on Biological Therapy*, *4*(5), 709-717. doi:10.1517/14712598.4.5.709

B Carvalho, S., Fortuna, A. R., Wolff, M. W., Peixoto, C., M Alves, P., Reichl, U., & JT Carrondo, M. (2018). Purification of influenza virus-like particles using sulfated cellulose membrane adsorbers. *Journal of Chemical Technology & Biotechnology*, *93*(7), 1988-1996. doi:10.1002/jctb.5474

Baek, J.-O., Seo, J.-W., Kim, I.-H., & Kim, C. H. (2011). Production and purification of human papillomavirus type 33 L1 virus-like particles from Spodoptera frugiperda 9 cells using two-step column chromatography. *Protein Expr Purif*, *75*(2), 211-217. doi:https://doi.org/10.1016/j.pep.2010.08.005

Barr, I. G., Donis, R. O., Katz, J. M., McCauley, J. W., Odagiri, T., Trusheim, H., . . . Wentworth, D. E. (2018). Cell culture-derived influenza vaccines in the severe 2017-2018 epidemic season: a step towards improved influenza vaccine effectiveness. *NPJ Vaccines*, *3*, 44-44. doi:10.1038/s41541-018-0079-z

Bissinger, T., Fritsch, J., Mihut, A., Wu, Y., Liu, X., Genzel, Y., . . . Reichl, U. (2019). Semi-perfusion cultures of suspension MDCK cells enable high cell concentrations and efficient influenza A virus production. *Vaccine*. doi:10.1016/j.vaccine.2019.04.054

Bock, A., Schulze-Horsel, J., Schwarzer, J., Rapp, E., Genzel, Y., & Reichl, U. (2011). High-density microcarrier cell cultures for influenza virus production. *Biotechnol Prog*, *27*(1), 241-250. doi:doi:10.1002/btpr.539

Bresee, J. S., Fry, A. M., Sambhara, S., & Cox, N. J. (2018). 31 - Inactivated Influenza Vaccines. In S. A. Plotkin, W. A. Orenstein, P. A. Offit, & K. M. Edwards (Eds.), *Plotkin's Vaccines (Seventh Edition)* (pp. 456-488.e421): Elsevier.

Bron, R., Ortiz, A., Dijkstra, J., Stegmann, T., & Wilschut, J. (1993). [23] Preparation, properties, and applications of reconstituted influenza virus envelopes (virosomes). In *Methods in Enzymology* (Vol. 220, pp. 313-331): Academic Press.

Castro, R., Fernandes, P., Laske, T., Sousa, M. F. Q., Genzel, Y., Scharfenberg, K., . . . Coroadinha, A. S. (2015). Production of canine adenovirus type 2 in serum-free suspension cultures of MDCK cells. *Appl Microbiol Biotechnol*, *99*(17), 7059-7068. doi:10.1007/s00253-015-6636-8

CDC. (2020, 06.01.2020). Clinical Update Announcement: Temporary Total Depletion of US Licensed Yellow Fever Vaccine Addressed by Availability of Stamaril Vaccine at Selected Clinics. Retrieved from https://wwwnc.cdc.gov/travel/news-announcements/yellow-fever-vaccine-access

Christie, A., & Butler, M. (1999). The adaptation of bhk cells to a non-ammoniagenic glutamate-based culture medium. *Biotechnol Bioeng*, *64*(3), 298-309. doi:10.1002/(sici)1097-0290(19990805)64:3<298::Aid-bit6>3.0.Co;2-u

. Chromatographic Purification of Virus Particles. In *Encyclopedia of Industrial Biotechnology* (pp. 1-21).

Chu, C., Lugovtsev, V., Golding, H., Betenbaugh, M., & Shiloach, J. (2009). Conversion of MDCK cell line to suspension culture by transfecting with human siat7e gene and its application for influenza virus production. *Proceedings of the National Academy of Sciences*, *106*(35), 14802-14807. doi:10.1073/pnas.0905912106

752 Coronel, J., Behrendt, I., Bürgin, T., Anderlei, T., Sandig, V., Reichl, U., & Genzel, Y. (2019). Influenza A
753 virus production in a single-use orbital shaken bioreactor with ATF or TFF perfusion systems.
754 *Vaccine*. doi:10.1016/j.vaccine.2019.06.005
755 Cusi, M. G. (2006). Applications of Influenza Virosomes as a Delivery System. *Human Vaccines*, *2*(1),
756 1-7. doi:10.4161/hv.2.1.2494
757 Doroshenko, A., & Halperin, S. A. (2009). Trivalent MDCK cell culture-derived influenza vaccine
758 Optaflu® (Novartis Vaccines). *Expert Review of Vaccines*, *8*(6), 679-688.
759 doi:10.1586/erv.09.31
760 Dukes, J. D., Whitley, P., & Chalmers, A. D. (2011). The MDCK variety pack: choosing the right strain.
761 *BMC Cell Biology*, *12*(1), 43. doi:10.1186/1471-2121-12-43
762 Eagle, H. (1959). Amino Acid Metabolism in Mammalian Cell Cultures. *Science*, *130*(3373), 432-437.
763 doi:10.1126/science.130.3373.432
764 Ernest, M., & Kamen, A. A. (2015). Current and Emerging Cell Culture Manufacturing Technologies for
765 Influenza Vaccines. *BioMed Research International*, *2015*, 11. doi:10.1155/2015/504831
766 Ferguson, N. M., Cummings, D. A. T., Fraser, C., Cajka, J. C., Cooley, P. C., & Burke, D. S. (2006).
767 Strategies for mitigating an influenza pandemic. *Nature*, *442*, 448. doi:10.1038/nature04795

768 https://www.nature.com/articles/nature04795#supplementary-information
769 Fineberg, H. V. (2014). Pandemic Preparedness and Response — Lessons from the H1N1 Influenza of
770 2009. *New England Journal of Medicine*, *370*(14), 1335-1342. doi:10.1056/NEJMra1208802
771 Fortuna, A. R., Taft, F., Villain, L., Wolff, M. W., & Reichl, U. (2018). Optimization of cell culture-
772 derived influenza A virus particles purification using sulfated cellulose membrane adsorbers.
773 *Engineering in Life Sciences*, *18*(1), 29-39. doi:10.1002/elsc.201700108
774 Fortuna, R. A., van Teeffelen, S., Ley, A., Fischer, L. M., Taft, F., Genzel, Y., . . . Reichl, U. (2019). Use of
775 sulfated cellulose membrane adsorbers for chromatographic purification of cell cultured-
776 derived influenza A and B viruses. *Separation and Purification Technology*.
777 doi:10.1016/j.seppur.2019.05.101
778 Frensing, T., Kupke, S. Y., Bachmann, M., Fritzsche, S., Gallo-Ramirez, L. E., & Reichl, U. (2016).
779 Influenza virus intracellular replication dynamics, release kinetics, and particle morphology
780 during propagation in MDCK cells. *Appl Microbiol Biotechnol*, *100*(16), 7181-7192.
781 doi:10.1007/s00253-016-7542-4
782 Freund, N. W., & Croughan, M. S. (2018). A Simple Method to Reduce both Lactic Acid and
783 Ammonium Production in Industrial Animal Cell Culture. *International Journal of Molecular*
784 *Sciences*, *19*(2), 385.
785 Gagnon, M., Hiller, G., Luan, Y.-T., Kittredge, A., DeFelice, J., & Drapeau, D. (2011). High-End pH-
786 controlled delivery of glucose effectively suppresses lactate accumulation in CHO Fed-batch
787 cultures. *Biotechnol Bioeng*, *108*(6), 1328-1337. doi:10.1002/bit.23072
788 Gagnon, P. (2009). Chromatographic Purification of Virus Particles. In *Encyclopedia of Industrial*
789 *Biotechnology* (pp. 1-21).
790 Gagnon, P., Nian, R., Tan, L., Cheong, J., Yeo, V., Yang, Y., & Gan, H. T. (2014). Chromatin-mediated
791 depression of fractionation performance on electronegative multimodal chromatography
792 media, its prevention, and ramifications for purification of immunoglobulin G. *Journal of*
793 *Chromatography A*, *1374*, 145-155. doi:https://doi.org/10.1016/j.chroma.2014.11.052
794 Gagnon, P., Nian, R., Yang, Y., Yang, Q., & Lim, C. L. (2015). Non-immunospecific association of
795 immunoglobulin G with chromatin during elution from protein A inflates host contamination,
796 aggregate content, and antibody loss. *Journal of Chromatography A*, *1408*, 151-160.
797 doi:https://doi.org/10.1016/j.chroma.2015.07.017
798 Gallo-Ramirez, L. E., Nikolay, A., Genzel, Y., & Reichl, U. (2015). Bioreactor concepts for cell culture-
799 based viral vaccine production. *Expert Rev Vaccines*, *14*(9), 1181-1195.
800 doi:10.1586/14760584.2015.1067144
801 Genzel, Y., Fischer, M., & Reichl, U. (2006). Serum-free influenza virus production avoiding washing
802 steps and medium exchange in large-scale microcarrier culture. *Vaccine*, *24*(16), 3261-3272.
803 doi:10.1016/j.vaccine.2006.01.019

Genzel, Y., Olmer, R. M., Schäfer, B., & Reichl, U. (2006). Wave microcarrier cultivation of MDCK cells for influenza virus production in serum containing and serum-free media. *Vaccine*, *24*(35), 6074-6087. doi:10.1016/j.vaccine.2006.05.023

Genzel, Y., & Reichl, U. (2007). Vaccine Production. In R. Pörtner (Ed.), *Animal Cell Biotechnology: Methods and Protocols* (pp. 457-473). Totowa, NJ: Humana Press.

Genzel, Y., & Reichl, U. (2009). Continuous cell lines as a production system for influenza vaccines. *Expert Review of Vaccines*, *8*(12), 1681-1692. doi:10.1586/erv.09.128

Genzel, Y., Ritter, J. B., König, S., Alt, R., & Reichl, U. (2005). Substitution of Glutamine by Pyruvate To Reduce Ammonia Formation and Growth Inhibition of Mammalian Cells. *Biotechnol Prog*, *21*(1), 58-69. doi:10.1021/bp049827d

George, M., Farooq, M., Dang, T., Cortes, B., Liu, J., & Maranga, L. (2010). Production of cell culture (MDCK) derived live attenuated influenza vaccine (LAIV) in a fully disposable platform process. *Biotechnol Bioeng*, *106*(6), 906-917. doi:doi:10.1002/bit.22753

Girard, M. P., Tam, J. S., Assossou, O. M., & Kieny, M. P. (2010). The 2009 A (H1N1) influenza virus pandemic: A review. *Vaccine*, *28*(31), 4895-4902. doi:https://doi.org/10.1016/j.vaccine.2010.05.031

Gregersen, J.-P., Schmitt, H.-J., Trusheim, H., & Bröker, M. (2011). Safety of MDCK cell culture-based influenza vaccines. *Future Microbiology*, *6*(2), 143-152. doi:10.2217/fmb.10.161

Horimoto, T., & Kawaoka, Y. (2001). Pandemic Threat Posed by Avian Influenza A Viruses. *Clinical Microbiology Reviews*, *14*(1), 129-149. doi:10.1128/cmr.14.1.129-149.2001

Hu, A. Y.-C., Tseng, Y.-F., Weng, T.-C., Liao, C.-C., Wu, J., Chou, A.-H., . . . Chong, P. (2011). Production of Inactivated Influenza H5N1 Vaccines from MDCK Cells in Serum-Free Medium. *PLoS One*, *6*(1), e14578. doi:10.1371/journal.pone.0014578

Hu, A. Y.-C., Weng, T.-C., Tseng, Y.-F., Chen, Y.-S., Wu, C.-H., Hsiao, S., . . . Lee, M.-S. (2008). Microcarrier-based MDCK cell culture system for the production of influenza H5N1 vaccines. *Vaccine*, *26*(45), 5736-5740. doi:https://doi.org/10.1016/j.vaccine.2008.08.015

Huang, D., Peng, W. J., Ye, Q., Liu, X. P., Zhao, L., Fan, L., . . . Tan, W. S. (2015). Serum-Free Suspension Culture of MDCK Cells for Production of Influenza H1N1 Vaccines. *PLoS One*, *10*(11), e0141686. doi:10.1371/journal.pone.0141686

Huang, D., Zhao, L., & Tan, W. (2011). Adherent and single-cell suspension culture of Madin-Darby canine kidney cells in serum-free medium. *Sheng wu gong cheng xue bao = Chinese journal of biotechnology*, *27*(4), 645-652.

Ikeda, Y., Iwakiri, S., & Yoshimori, T. (2009). Development and characterization of a novel host cell DNA assay using ultra-sensitive fluorescent nucleic acid stain “PicoGreen”. *Journal of Pharmaceutical and Biomedical Analysis*, *49*(4), 997-1002. doi:https://doi.org/10.1016/j.jpba.2009.01.022

Jin, H., & Subbarao, K. (2015). Live Attenuated Influenza Vaccine. In M. B. A. Oldstone & R. W. Compans (Eds.), *Influenza Pathogenesis and Control - Volume II* (pp. 181-204). Cham: Springer International Publishing.

Kalbfuss, B., Knöchlein, A., Kröber, T., & Reichl, U. (2008). Monitoring influenza virus content in vaccine production: Precise assays for the quantitation of hemagglutination and neuraminidase activity. *Biologicals*, *36*(3), 145-161. doi:https://doi.org/10.1016/j.biologicals.2007.10.002

Kärber, G. (1931). Beitrag zur kollektiven Behandlung pharmakologischer Reihenversuche. *Naunyn-Schmiedebergs Archiv für experimentelle Pathologie und Pharmakologie*, *162*(4), 480-483. doi:10.1007/bf01863914

Kilbourne, E. D. (2006). Influenza pandemics of the 20th century. *Emerg Infect Dis*, *12*(1), 9-14. doi:10.3201/eid1201.051254

Kostova, D., Reed, C., Finelli, L., Cheng, P.-Y., Gargiullo, P. M., Shay, D. K., . . . Bresee, J. S. (2013). Influenza Illness and Hospitalizations Averted by Influenza Vaccination in the United States, 2005–2011. *PLoS One*, *8*(6), e66312. doi:10.1371/journal.pone.0066312

Kröber, T., Wolff, M. W., Hundt, B., Seidel-Morgenstern, A., & Reichl, U. (2013). Continuous purification of influenza virus using simulated moving bed chromatography. *Journal of Chromatography A*, *1307*, 99-110. doi:https://doi.org/10.1016/j.chroma.2013.07.081

Kuiper, M., Sanches, R. M., Walford, J. A., & Slater, N. K. H. (2002). Purification of a functional gene therapy vector derived from Moloney murine leukaemia virus using membrane filtration and ceramic hydroxyapatite chromatography. *Biotechnol Bioeng*, *80*(4), 445-453. doi:10.1002/bit.10388

Le Ru, A., Jacob, D., Transfiguracion, J., Ansorge, S., Henry, O., & Kamen, A. A. (2010). Scalable production of influenza virus in HEK-293 cells for efficient vaccine manufacturing. *Vaccine*, *28*(21), 3661-3671. doi:10.1016/j.vaccine.2010.03.029

Lee, M. F. X., Chan, E. S., Tan, W. S., Tam, K. C., & Tey, B. T. (2015). Negative chromatography purification of hepatitis B virus-like particles using poly(oligo(ethylene glycol) methacrylate) grafted cationic adsorbent. *Journal of Chromatography A*, *1415*, 161-165. doi:https://doi.org/10.1016/j.chroma.2015.08.056

Li, H., Yang, Y., Zhang, Y., Zhang, S., Zhao, Q., Zhu, Y., . . . Su, Z. (2015). A hydrophobic interaction chromatography strategy for purification of inactivated foot-and-mouth disease virus. *Protein Expr Purif*, *113*, 23-29. doi:https://doi.org/10.1016/j.pep.2015.04.011

Li, K. S., Guan, Y., Wang, J., Smith, G. J. D., Xu, K. M., Duan, L., . . . Peiris, J. S. M. (2004). Genesis of a highly pathogenic and potentially pandemic H5N1 influenza virus in eastern Asia. *Nature*, *430*, 209. doi:10.1038/nature02746

https://www.nature.com/articles/nature02746#supplementary-information

Ljunggren, J., & Häggström, L. (1994). Catabolic control of hybridoma cells by glucose and glutamine limited fed batch cultures. *Biotechnol Bioeng*, *44*(7), 808-818. doi:10.1002/bit.260440706

Lohr, V., Genzel, Y., Behrendt, I., Scharfenberg, K., & Reichl, U. (2010). A new MDCK suspension line cultivated in a fully defined medium in stirred-tank and wave bioreactor. *Vaccine*, *28*(38), 6256-6264. doi:10.1016/j.vaccine.2010.07.004

Lopes, A. G. (2015). Single-use in the biopharmaceutical industry: A review of current technology impact, challenges and limitations. *Food and Bioproducts Processing*, *93*, 98-114. doi:https://doi.org/10.1016/j.fbp.2013.12.002

Maranga, L., & Goochee, C. F. (2006). Metabolism of PER.C6TM cells cultivated under fed-batch conditions at low glucose and glutamine levels. *Biotechnol Bioeng*, *94*(1), 139-150. doi:10.1002/bit.20890

Marichal-Gallardo, P., Pieler, M. M., Wolff, M. W., & Reichl, U. (2017). Steric exclusion chromatography for purification of cell culture-derived influenza A virus using regenerated cellulose membranes and polyethylene glycol. *Journal of Chromatography A*, *1483*, 110-119. doi:10.1016/j.chroma.2016.12.076

Milián, E., Julien, T., Biaggio, R., Venereo-Sanchez, A., Montes, J., Manceur, A. P., . . . Kamen, A. (2017). Accelerated mass production of influenza virus seed stocks in HEK-293 suspension cell cultures by reverse genetics. *Vaccine*, *35*(26), 3423-3430. doi:https://doi.org/10.1016/j.vaccine.2017.04.065

Momose, F., Kikuchi, Y., Komase, K., & Morikawa, Y. (2007). Visualization of microtubule-mediated transport of influenza viral progeny ribonucleoprotein. *Microbes and Infection*, *9*(12), 1422-1433. doi:10.1016/j.micinf.2007.07.007

Montomoli, E., Khadang, B., Piccirella, S., Trombetta, C., Mennitto, E., Manini, I., . . . Lapini, G. (2012). Cell culture-derived influenza vaccines from Vero cells: a new horizon for vaccine production. *Expert Review of Vaccines*, *11*(5), 587-594. doi:10.1586/erv.12.24

Morenweiser, R. (2005). Downstream processing of viral vectors and vaccines. *Gene Therapy*, *12*, S103. doi:10.1038/sj.gt.3302624

Nian, R., & Gagnon, P. (2016). Advance chromatin extraction enhances performance and productivity of cation exchange chromatography-based capture of Immunoglobulin G monoclonal antibodies. *Journal of Chromatography A*, *1453*, 54-61. doi:https://doi.org/10.1016/j.chroma.2016.05.029

Onions, D., Egan, W., Jarrett, R., Novicki, D., & Gregersen, J.-P. (2010). Validation of the safety of MDCK cells as a substrate for the production of a cell-derived influenza vaccine. *Biologicals*, *38*(5), 544-551. doi:https://doi.org/10.1016/j.biologicals.2010.04.003

Opitz, L., Lehmann, S., Reichl, U., & Wolff, M. W. (2009). Sulfated membrane adsorbers for economic pseudo-affinity capture of influenza virus particles. *Biotechnol Bioeng*, *103*(6), 1144-1154. doi:10.1002/bit.22345

Peschel, B., Frentzel, S., Laske, T., Genzel, Y., & Reichl, U. (2013). Comparison of influenza virus yields and apoptosis-induction in an adherent and a suspension MDCK cell line. *Vaccine*, *31*(48), 5693-5699. doi:10.1016/j.vaccine.2013.09.051

Pieler, M. M., Heyse, A., Wolff, M. W., & Reichl, U. (2017). Specific ion effects on the particle size distributions of cell culture–derived influenza A virus particles within the Hofmeister series. *Engineering in Life Sciences*, *17*(5), 470-478. doi:10.1002/elsc.201600153

Raymond, D. D., Stewart, S. M., Lee, J., Ferdman, J., Bajic, G., Do, K. T., . . . Harrison, S. C. (2016). Influenza immunization elicits antibodies specific for an egg-adapted vaccine strain. *Nature Medicine*, *22*(12), 1465-1469. doi:10.1038/nm.4223

Ruining WANG, Y. Z., Junqing GUO,Qingmei LI,Li WANG,Jifei YANG,Qianyue JIN,Yinbiao WANG,Yanyan YANG,Guangxu XING,Songlin QIAO,Mengmeng ZHAO,Ruiguang DENG,Gaiping ZHANG. (2015). Efficient purification of cell culture-derived classical swine fever virus by ultrafiltration and size-exclusion chromatography. *Front. Agr. Sci. Eng.*, *2*(3), 230-236. doi:10.15302/j-fase-2015071

Schild, G. C., Oxford, J. S., de Jong, J. C., & Webster, R. G. (1983). Evidence for host-cell selection of influenza virus antigenic variants. *Nature*, *303*(5919), 706-709. doi:10.1038/303706a0

Schneider, M., Marison, I. W., & von Stockar, U. (1996). The importance of ammonia in mammalian cell culture. *J Biotechnol*, *46*(3), 161-185. doi:10.1016/0168-1656(95)00196-4

Singer, V. L., Jones, L. J., Yue, S. T., & Haugland, R. P. (1997). Characterization of PicoGreen Reagent and Development of a Fluorescence-Based Solution Assay for Double-Stranded DNA Quantitation. *Anal Biochem*, *249*(2), 228-238. doi:https://doi.org/10.1006/abio.1997.2177

Skowronski, D. M., Janjua, N. Z., De Serres, G., Sabaiduc, S., Eshaghi, A., Dickinson, J. A., . . . Li, Y. (2014). Low 2012–13 Influenza Vaccine Effectiveness Associated with Mutation in the Egg-Adapted H3N2 Vaccine Strain Not Antigenic Drift in Circulating Viruses. *PLoS One*, *9*(3), e92153. doi:10.1371/journal.pone.0092153

Slivac, I., Blajić, V., Radošević, K., Kniewald, Z., & Gaurina Srček, V. (2010). Influence of different ammonium, lactate and glutamine concentrations on CCO cell growth. *Cytotechnology*, *62*(6), 585-594. doi:10.1007/s10616-010-9312-y

Spearman, C. (1909). Review of The Method of 'Right and Wrong Cases' ('Constant Stimuli') without Gauss's Formula. *Psychological Bulletin*, *6*(1), 27-28. doi:10.1037/h0063767

Tan, L., Yeo, V., Yang, Y., & Gagnon, P. (2015). Characterization of DNA in cell culture supernatant by fluorescence-detection size-exclusion chromatography. *Anal Bioanal Chem*, *407*(14), 4173-4181. doi:10.1007/s00216-015-8639-9

Tree, J. A., Richardson, C., Fooks, A. R., Clegg, J. C., & Looby, D. (2001). Comparison of large-scale mammalian cell culture systems with egg culture for the production of influenza virus A vaccine strains. *Vaccine*, *19*(25), 3444-3450. doi:10.1016/S0264-410X(01)00053-6

Vajda, J., Weber, D., Stefaniak, S., Hundt, B., Rathfelder, T., & Müller, E. (2016). Mono- and polyprotic buffer systems in anion exchange chromatography of influenza virus particles. *Journal of Chromatography A*, *1448*, 73-80. doi:https://doi.org/10.1016/j.chroma.2016.04.047

van Wielink, R., Kant-Eenbergen, H. C. M., Harmsen, M. M., Martens, D. E., Wijffels, R. H., & Coco-Martin, J. M. (2011). Adaptation of a Madin–Darby canine kidney cell line to suspension growth in serum-free media and comparison of its ability to produce avian influenza virus to Vero and BHK21 cell lines. *Journal of Virological Methods*, *171*(1), 53-60. doi:10.1016/j.jviromet.2010.09.029

Wang, H., Guo, S., Li, Z., Xu, X., Shao, Z., & Song, G. (2017). Suspension culture process for H9N2 avian influenza virus (strain Re-2). *Archives of Virology*, *162*(10), 3051-3059. doi:10.1007/s00705-017-3460-8

Webby, R. J., & Webster, R. G. (2003). Are We Ready for Pandemic Influenza? *Science*, *302*(5650), 1519-1522. doi:10.1126/science.1090350

Weigel, T., Solomaier, T., Wehmeyer, S., Peuker, A., Wolff, M. W., & Reichl, U. (2016). A membrane-based purification process for cell culture-derived influenza A virus. *J Biotechnol*, *220*, 12-20. doi:https://doi.org/10.1016/j.jbiotec.2015.12.022

Wolf, M. W., & Reichl, U. (2011). Downstream processing of cell culture-derived virus particles. *Expert Review of Vaccines*, *10*(10), 1451-1475. doi:10.1586/erv.11.111

Wolff, M. W., & Reichl, U. (2008). Downstream Processing: From Egg to Cell Culture-Derived Influenza Virus Particles. *Chemical Engineering & Technology*, *31*(6), 846-857. doi:doi:10.1002/ceat.200800118

Wolff, M. W., Siewert, C., Hansen, S. P., Faber, R., & Reichl, U. (2010). Purification of cell culture-derived modified vaccinia ankara virus by pseudo-affinity membrane adsorbers and hydrophobic interaction chromatography. *Biotechnol Bioeng*, *107*(2), 312-320. doi:10.1002/bit.22797

Wood, J. M., Schild, G. C., Newman, R. W., & Seagroatt, V. (1977). An improved single-radial-immunodiffusion technique for the assay of influenza haemagglutinin antigen: application for potency determinations of inactivated whole virus and subunit vaccines. *J Biol Stand*, *5*(3), 237-247.

Wu, N. C., Zost, S. J., Thompson, A. J., Oyen, D., Nycholat, C. M., McBride, R., . . . Wilson, I. A. (2017). A structural explanation for the low effectiveness of the seasonal influenza H3N2 vaccine. *PLoS Pathogens*, *13*(10), e1006682. doi:10.1371/journal.ppat.1006682

Zost, S. J., Parkhouse, K., Gumina, M. E., Kim, K., Diaz Perez, S., Wilson, P. C., . . . Hensley, S. E. (2017). Contemporary H3N2 influenza viruses have a glycosylation site that alters binding of antibodies elicited by egg-adapted vaccine strains. *Proceedings of the National Academy of Sciences*, *114*(47), 12578-12583. doi:10.1073/pnas.1712377114